Journal of Alloys and Compounds 509 (2011) 8268–8275

Contents lists available at ScienceDirect

Journal of Alloys and Compounds

journal homepage: www.elsevier.com/locate/jallcom

Double-peak ageing behavior of Mg–2Dy–0.5Zn alloy

Guangli Bi, Daqing Fang, Lei Zhao, Qingxin Zhang, Jianshe Lian, Qing Jiang, Zhonghao Jiang*

Key Laboratory of Automobile Materials, College of Materials Science and Engineering, Jilin University, Nanling Campus, Changchun 130025, China

ARTICLE INFO

Article history:
Received 19 December 2010
Received in revised form 25 May 2011
Accepted 31 May 2011
Available online 6 June 2011

Keywords:
Magnesium alloy
Mg–Dy–Zn alloy
Ageing behavior
Long period stacking ordered phase
Precipitation strengthening

ABSTRACT

Ageing behavior of Mg–2Dy–0.5Zn alloy was investigated during isothermal ageing at 180 °C. Two significant ageing peaks were observed at 36 h and 80 h, respectively. Examination of microstructure evolution during ageing revealed that 14H long period stacking ordered (LPSO) phase forms in the α-Mg matrix and its volume fraction increases, $(Mg, Zn)_xDy$ particle phases precipitate and their size, distribution and amount vary, as ageing time increases. The LPSO strengthening and the precipitation strengthening are two main mechanisms responsible for the double-peak ageing behavior observed for the Mg–2Dy–0.5Zn alloy. The first ageing peak is mainly attributed to the precipitation strengthening of a large amount of the fine $(Mg, Zn)_xDy$ particle phases. The second ageing peak arises mainly from the LPSO strengthening of a high volume fraction of the 14H LPSO phase.

1. Introduction

From the view of energy saving and environment protection, light weight of metallic structural materials is becoming increasingly important. Magnesium alloys, as the lightest metallic materials, have received considerable interest in recent years because of their low density, high stiffness and high specific strength [1,2]. However, low tensile strengths and poor heat resistant properties limit the applications of Mg alloys at high temperature fields. The investigations [3–14] have demonstrated that the combination addition of one/two kinds of rare earth (RE) elements (especially heavy RE elements such as Y, Gd and Dy) and Zn elements can effectively improve strengths of Mg–RE–Zn alloys at room temperature and elevated temperatures through significant precipitation strengthening and long period stacking ordered (LPSO) phase strengthening.

The investigations on the ageing behavior of Mg–RE–Zn alloys [15–17] have shown that the precipitation of coherent and non-coherent Mg–RE particle phases and the formation of LPSO phases in the supersaturated α-Mg solid solution play a dominant role in enhancing ageing hardening response during isothermal ageing. Honma et al.'s study on the ageing behavior of Mg–2.0Gd–1.2Y–1Zn–0.2Zr (at.%) alloy at 225 °C [15] revealed that the concurrent precipitations of the β′ (bco) and β_1 (fcc) particle phases lead to a significant ageing peak at 32 h and the 14H LPSO phase forms in the over-raged condition (288 h). Yamasaki et al.'s investigation of the ageing behavior of $Mg_{97}Gd_2Zn_1$ (at.%) alloy at temperature range from 200 °C to 500 °C [16] showed that a significant ageing peak occurs at 200 °C due to the precipitation of the β′ (orthor, Mg_7Gd) particle phases, while 14H LPSO phases form at 350–500 °C and result only in a limited ageing hardening response. Liu et al. [17] reported that during the ageing of an extruded Mg–7Y–4Gd–0.5Zn–0.4Zr alloy at 250 °C, both β′ (cbco) and 14H LPSO phases coexist together and contribute to the peak ageing hardening response of this alloy at 80 h.

From the above investigations of the ageing behaviors of the Mg–Y(Gd)–Zn alloys, it can be noted that these alloys exhibit always a single peak ageing behavior and this ageing behavior arises mainly from the precipitation strengthening of the β′ phases. The 14H LPSO phase forms and develops during ageing at different time and temperature, but its contribution to the ageing hardening responses of these alloys is not very significant due to its limited amount. On the other hand, recently many researchers have reported the phase structure and transformation of Mg–Y(Gd)–Zn(Ni, Cu) alloys with LPSO phase in the heat-treated state [18], the rapidly solidified state [19,20] and the aged state [21]. However, the ageing behavior and corresponding phase transformation of the Mg–Dy–Zn alloy during ageing are not investigated up to date. Therefore, in this study, we prepared a Mg–2Dy–0.5Zn (at.%) alloy and investigated its ageing behavior during isothermal ageing at 180 °C and the corresponding microstructure evolution, especially the formation and development of 14H LPSO phase and its contribution to the ageing hardening response of this alloy.

2. Experimental procedures

Mg–2Dy–0.5Zn (at.%) alloy was prepared from high pure Mg and pure Zn and Mg–20Dy (wt.%) master alloy. Melting was conducted by using a graphite crucible in an electric resistance furnace at about 750 °C under the protection of antioxidant

* Corresponding author. Fax: +86 431 8509 5876.
E-mail address: jzh@jlu.edu.cn (Z. Jiang).

0925-8388/$ – see front matter © 2011 Elsevier B.V. All rights reserved.
doi:10.1016/j.jallcom.2011.05.117

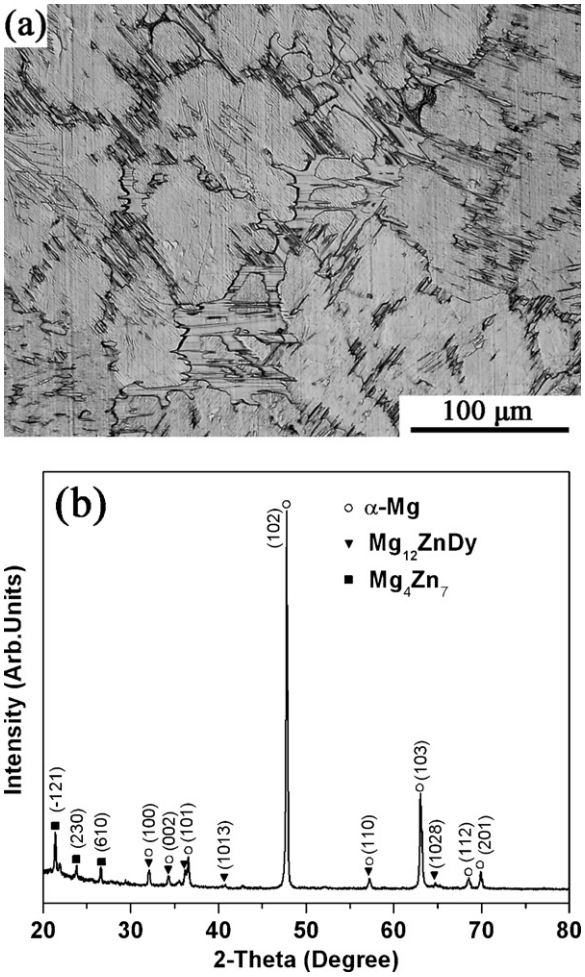

Fig. 1. Optical microstructure (a) and corresponding XRD pattern (b) of the as-cast Mg–2Dy–0.5Zn alloy.

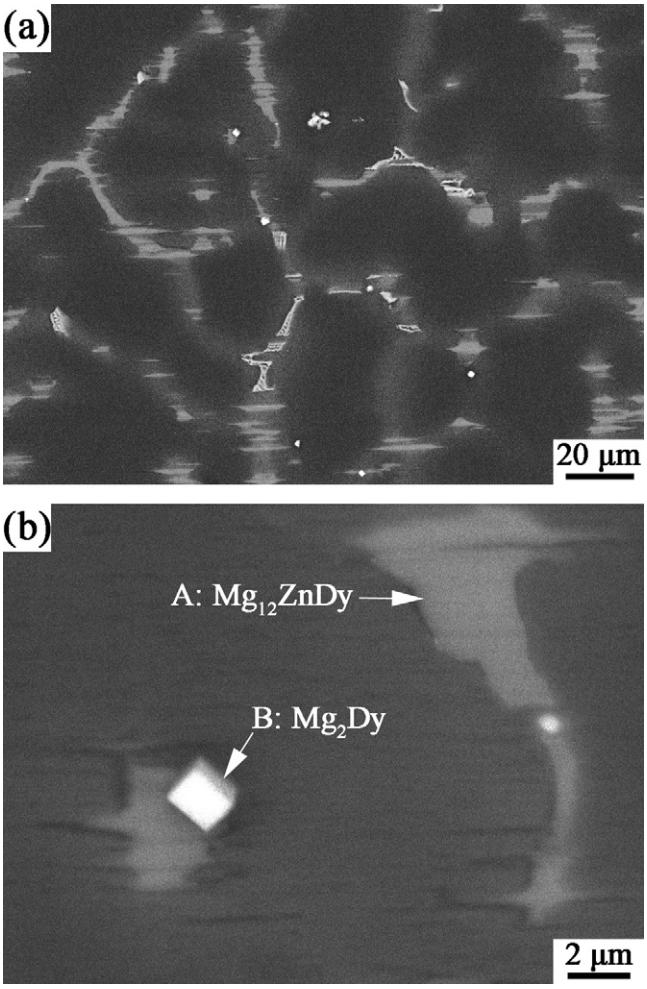

Fig. 2. SEM images of the as-cast Mg–2Dy–0.5Zn alloy in low magnification (a) and high magnification (b).

flux. The melts were homogenized at 720 °C for 0.5 h, and then cast into a steel mould with size of 70 mm × 40 mm × 13 mm. Some of the ingots were solid-solution treated at 525 °C for 10 h and then quenched into water at room temperature. These treated ingots were finally aged at 180 °C for 128 h.

Microstructures, phase structure and phase composition of the alloy were characterized using optical microscope (Olympus GX71), X-ray diffraction (XRD) (Rigaku D/max 2500PC), scanning electron microscopy (SEM) (JSM-5600) equipped with X-ray energy-dispersive spectrometer (EDS) and transmission electronic microscopy (TEM) (JEM-2100F). The specimens for the optical and SEM observations were ground, polished and etched in a picric acid–ethanol–H_2O solution. The thin foils for the TEM observation were prepared using Ion Polishing System (RES101). The hardness of the aged alloys was measured by a Vickers micro-hardness tester (FM-700) with load of 100 g and holding time of 15 s. The hardness value of each aged sample was measured at least 20 points.

3. Results and discussion

3.1. Microstructures of the as-cast and solid-solution treated alloys

Fig. 1 shows the optical microstructure and corresponding XRD pattern of the as-cast Mg–2Dy–0.5Zn alloy. As shown in Fig. 1(a), the microstructure of the as-cast alloy is mainly composed of α-Mg matrix and coarse lamellar phases that distribute at the grain boundaries and in the grain interior. The corresponding XRD pattern in Fig. 1(b) reveals that besides the α-Mg phase, there exist the Mg_4Zn_7 and $Mg_{12}ZnDy$ phases in the as-cast alloy. The $Mg_{12}ZnDy$ phase should have a similar crystalline structure with the $Mg_{12}ZnY$ phase in the Mg–Zn–Zr–Y alloy reported by Luo [22], because Dy and Y belong to the same subgroup and have similar atomic radius. Therefore, the atomic planes of the $Mg_{12}ZnDy$ phase revealed by the XRD pattern in Fig. 1(b) should be the same as those of the $Mg_{12}ZnY$ phase and thus are indexed according to the result of Luo [22]. Fig. 2 shows the SEM images of the as-cast alloy. The coarse lamellar phases with gray contrast and a small amount of the particle phases are observed in Fig. 2(a). The EDS analysis indicates that the average chemical composition of the lamellar phase as indicated by label A in Fig. 2(b) is Mg–6.24 at.% Dy–4.82 at.% Zn, indicating that the lamellar phase is the $Mg_{12}ZnDy$ phase with 18R LPSO structure. This EDS result is consistent with the XRD result. Such 18R LPSO phase has been commonly observed in the as-cast $Mg_{97}Zn_1Dy_2$ alloy [6] and $Mg_{97}Zn_1Y_2$ alloy [23]. The EDS analysis reveals that the average chemical composition of the square-shaped particle phase as indicated by label B in Fig. 2(b) is Mg–32.16 at.% Dy with the atomic ratio of Mg–Dy being about 2. Therefore, the formula of the square-shaped particle phase can be written as Mg_2Dy. This Mg_2Dy phase exists in the Mg–Dy system, but is not an equilibrium phase in our Mg–Dy–Zn system. This Mg_2Dy phase forms during solidification process due to the fluctuation or segregation of Dy and Zn and also the possible presence of the impurities such as hydrogen, oxygen or nitrogen, but does not take part actually in the phase transformation in solid-solution treatment and retains still in subsequent ageing treatment. Because of its small amount, this Mg_2Dy phase was not detected in the XRD pattern in Fig. 1(b).

Fig. 3 shows the optical microstructures and corresponding XRD pattern of the solid-solution treated alloy. After solid-solution

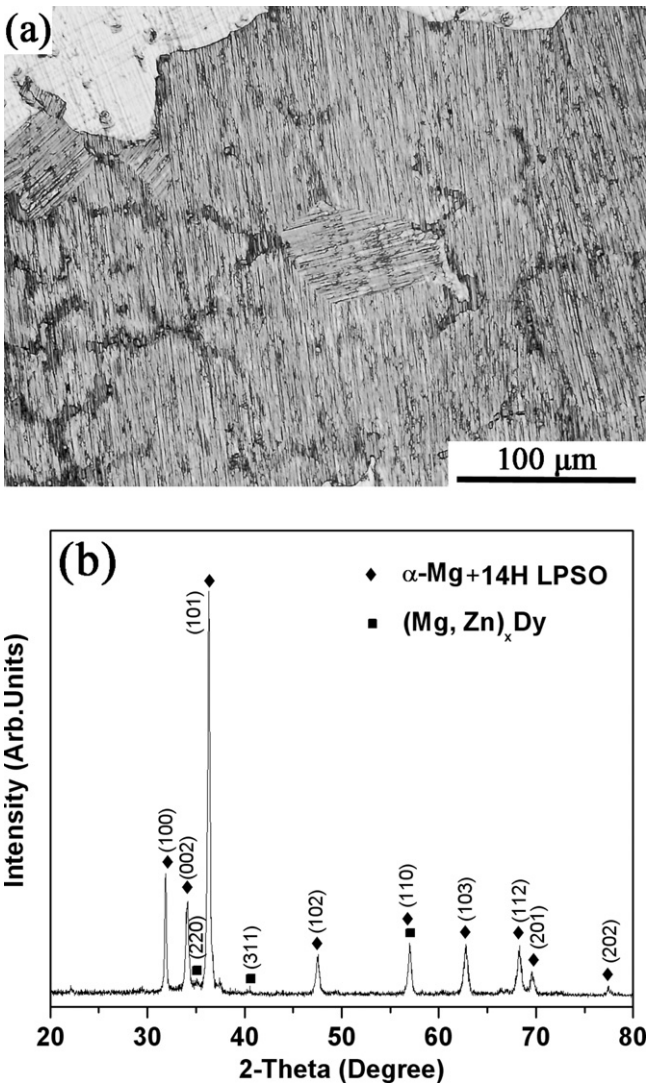

Fig. 3. Optical microstructure (a) and corresponding XRD pattern (b) of the solid-solution treated Mg–2Dy–0.5Zn alloy.

treatment at 525 °C for 10 h, the 18R LPSO phase formed during casting nearly disappears, the fine lamellar phase forms in all the grains and some irregular particle phases precipitate at the grain boundaries as shown in Fig. 3(a). As compared with the XRD pattern of the as-cast alloy, the diffraction peaks of the $Mg_{12}ZnDy$ phase disappear, new diffraction peaks of $(Mg, Zn)_xDy$ phase are detected in the XRD pattern of the solid-solution-treated alloy as seen in Fig. 3(b). It is noteworthy to mention that the intensities of the main diffraction peaks of the α-Mg phase increase significantly, which suggests that a new phase forms and this phase and the α-Mg matrix should have the same crystalline structure or similar lattice constant (hcp, $a = 0.3209$ nm and $c = 0.5211$ nm). The later TEM observation reveals that the fine lamellar phase in the grain interior is the 14H LPSO phase and the irregular particle phases are the $(Mg, Zn)_xDy$ phase. The $(Mg, Zn)_xDy$ particle phases form mainly along the original dendritic regions of the as-cast alloy. The grain coarsening role produced during solid-solution treatment would make the dendrites to be placed inside the grain interior. The higher concentrations of Dy and Zn richen in these regions in the grain interior would promote the precipitation of the $(Mg, Zn)_xDy$ particle phases during subsequent ageing treatment.

The formation of the 18R LPSO phase in the as-cast condition and the transformation of the 18R LPSO phase to the 14H LPSO phase

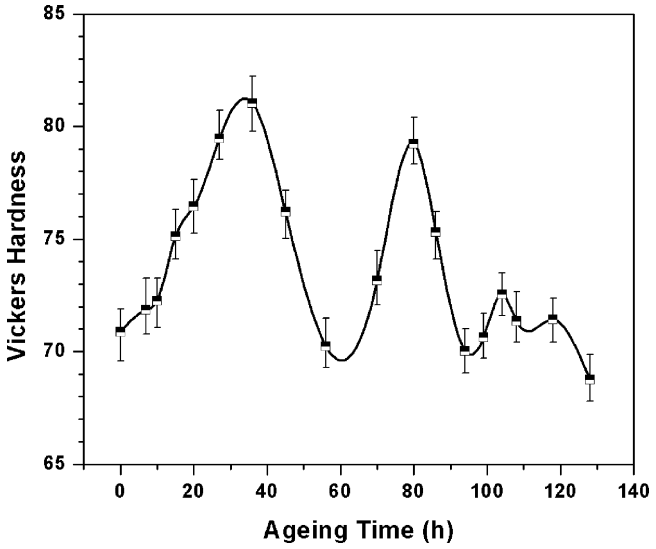

Fig. 4. Ageing hardening curves of the Mg–2Dy–0.5Zn alloy at 180 °C.

during solid-solution treatment in the Mg–2Dy–0.5Zn alloy should be related to atomic diffusion and segregation. During solidification process, the Dy atoms enriched at the solid/liquid interface would result in the composition super-cooling in the diffusion layer ahead the solid/liquid interface. The diffusion rates of the Dy and Zn atoms are thus reduced and most of the Dy and Zn atoms enrich eventually at the grain boundaries. When the chemical order and stacking order are satisfied, the 18R LPSO phase forms at the grain boundaries as shown in Fig. 1(a). During the subsequent solid-solution treatment, some Dy and Zn atoms diffuse from the $Mg_{12}DyZn$ (18R LPSO) phase to the α-Mg matrix, which would result in the formation of the fine lamellar 14H LPSO phase in the grain interior and would also promote the precipitation of the $(Mg, Zn)_xDy$ particle phases at the grain boundaries. In addition, because the melting point of 18R LPSO phase is not far from the solid-solution treatment temperature used in the present test, some small liquid zones enriched in Zn and Dy may exist and form the $(Mg, Zn)_xDy$ particle phases upon cooling. Furthermore, the transformation from the 18R LPSO phase to the 14H LPSO phase can be explained in terms of the minimization of the shear strain energy [24,25]. Both 18R LPSO and 14H LPSO phases are composed of the structure units that have a hexagonal structure with different stacking sequences of the closely packed plane [24]. The structure unit of the 18R LPSO phase contains three ABCA-type building blocks that arrange in the same shear direction and result in a shear strain with respect to the α-Mg matrix. In contrast, the structure unit of the 14H LPSO phase contains two ACBA-type building blocks that arrange in the opposite direction and do not create any shear strain. Therefore, the 18R LPSO phase is thermodynamically instable as compared with the 14H LPSO phase. During solid-solution treatment the 18R LPSO phase is gradually replaced by the 14H LPSO phase so as to relax high shear strain energy. So, the 18R LPSO phase was considered to be an elevated temperature phase and exists mainly in as-cast Mg–Zn–RE alloys [23], while the 14H LPSO phase was often observed in solid-solution treated Mg–Zn–RE alloys [6,23].

3.2. Ageing behavior of the heat treated alloy

Fig. 4 shows the ageing curves of the Mg–2Dy–0.5Zn alloy at 180 °C. It can be seen that the hardness is about 71 VHN at 0 h, then increases rapidly and reaches a maximum of 81 VHN at 36 h, which increases by 11% as compared with that at 0 h. After the peak hardness, the hardness begins to decrease and

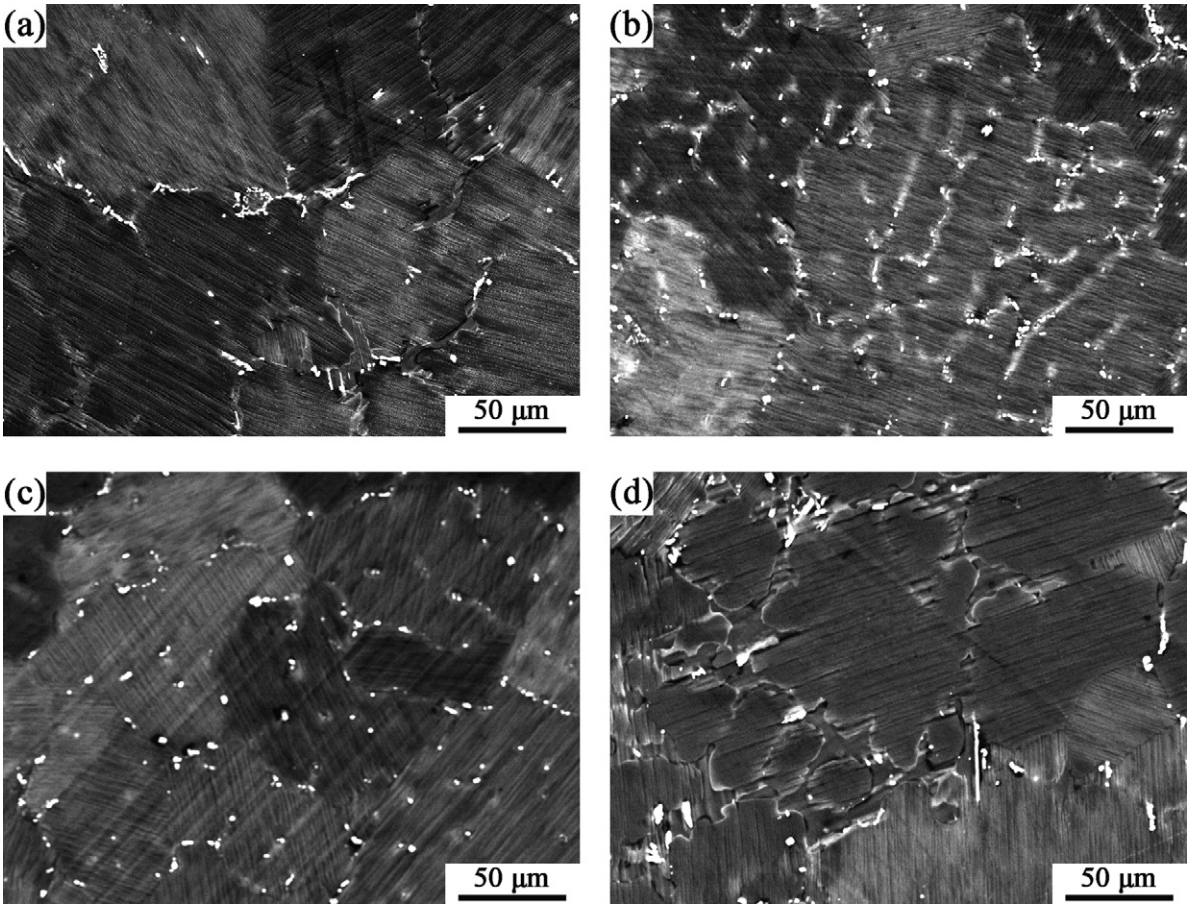

Fig. 5. SEM images of the aged Mg–2Dy–0.5Zn alloy at 0 h (a), 36 h (b), 80 h (c) and 128 h (d), respectively.

reaches to a minimum at 56 h. It is noted that the hardness increases again and reaches another maximum of 79 VHN at 80 h. This variation in hardness indicates that the Mg–2Dy–0.5Zn alloy exhibits a double-peak ageing behavior. Such double-peak ageing behavior was not observed in other Mg–RE–Zn alloys except in Mg–6Zn–5Al–*x*MM–*y*Sn ($x+y=4$ wt.%) alloy, where MM represents mischmetal [26]. The authors suggested that the double-peak ageing behavior observed in this alloy is related to the changes in the amount, distribution and morphology of the intermetallics including Al_2MMZn_2, $Mg_{32}(Al, Zn)_{49}$ and the Mg_2Sn phase during ageing.

3.3. Microstructure evolution of the aged alloy

Figs. 5 and 6 show the SEM images and corresponding XRD patterns of the aged Mg–2Dy–0.5Zn alloy at different ageing time. An important observation is that all the α-Mg grains are composed of the fine lamellar phases and show random orientations. The average grain size of the α-Mg phase remains unchanged except at 128 h where the α-Mg grains coarsen slightly. The white particle phases are observed and their size, distribution and amount vary significantly with ageing time. The white particle phases distribute mainly at the grain boundaries at 0 h and form gradually in the grain interior. As ageing time increases, the volume fraction of the particle phases increases significantly at 36 h as shown in Fig. 5(a) and (b). It is noted that narrow transition regions form in the vicinity of the white particle phases and become more evident at 36 h. Such transition regions have not been reported in other aged Mg alloys up to date. The transition regions shrink and disappear at 80 h. The white particle phases become coarse and distribute only in the grain boundaries at 128 h.

The corresponding XRD patterns of the aged alloy at six ageing time reveal that besides the diffraction peaks of the α-Mg matrix, the 14H LPSO phase and the $(Mg, Zn)_xDy$ phase, no new diffrac-

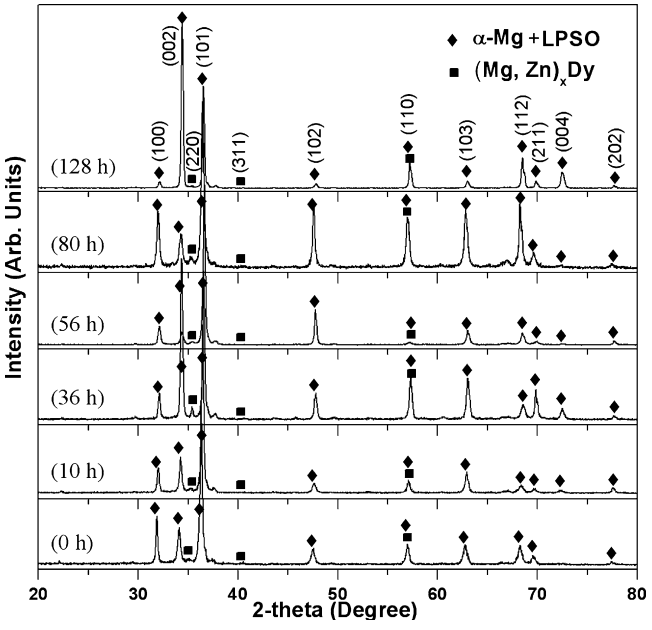

Fig. 6. XRD patterns of the Mg–2Dy–0.5Zn alloy at different ageing time.

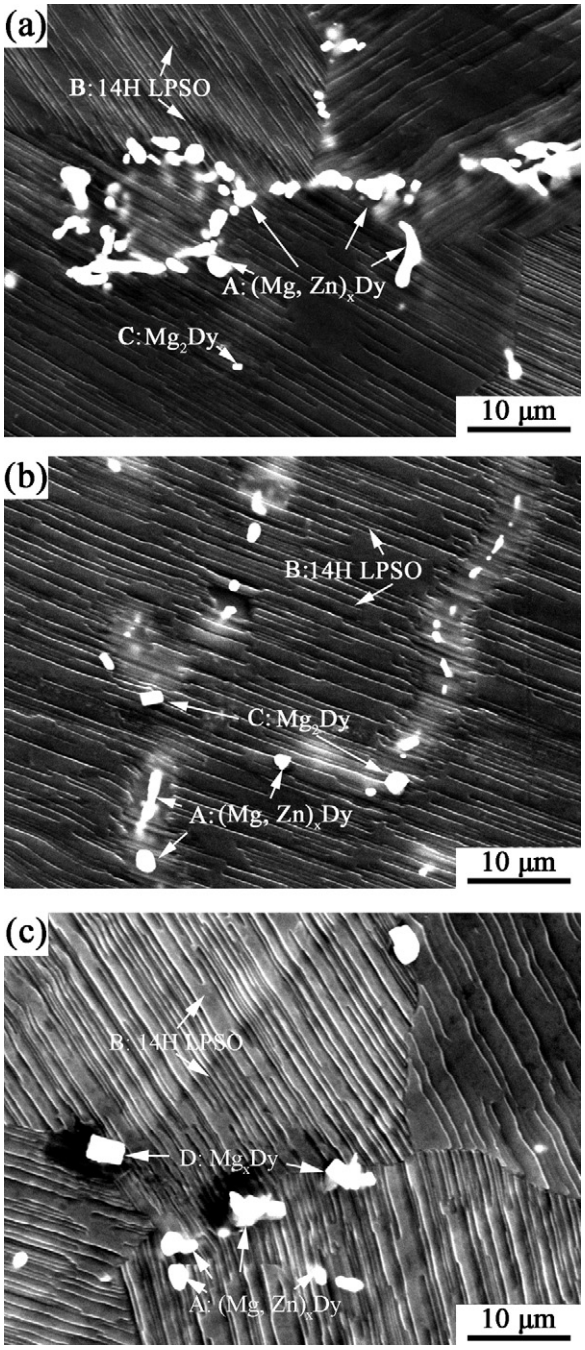

Fig. 7. SEM images of the aged Mg–2Dy–0.5Zn alloy at 0 h (a), 36 h (b) and 80 h (c), respectively.

tion peaks are detected. The intensity of the diffraction peak of the (Mg, Zn)$_x$Dy particle phases increases remarkably, reaches a maximum at 36 h and then decreases slightly as ageing time increases. Such change in the intensity of the diffraction peak of the (Mg, Zn)$_x$Dy particle phases is consistent with the change in their volume fraction.

In order to identify further the composition and structure of the white particle phases and the fine lamellar phase, the high resolution SEM images and corresponding EDS results of the aged alloy at 0 h, 36 h and 80 h are shown in Fig. 7 and Table 1, respectively. In all the SEM images, the white particle phases and fine lamellar phase are observed clearly in the α-Mg matrix. The white particle phases can be further classified into three types according to their morphologies, i.e., square-shaped, rectangular-shaped and irregular particle phases. Among them, the square-shaped and irregular particle phases exist consistently in the α-Mg matrix and are the Mg_2Dy phase and the (Mg, Zn)$_x$Dy phase with their average chemical compositions being Mg–33.26 at.% Dy and Mg–30.12 at.% Dy–39.23 at.% Zn, respectively, according to the EDS analysis. The rectangular-shaped particle phases precipitate at 80 h are the Mg$_x$Dy phase with its average chemical composition being Mg–28.73 at.% Dy according to the EDS analysis.

Fig. 8 displays the typical TEM images and corresponding selected area electron diffraction (SAED) patterns of the square-shaped and irregular particle phases in the aged Mg–2Dy–0.5Zn alloy at 36 h. The SAED patterns of these two particle phases in Fig. 8(b) and (c) show that the square-shaped Mg_2Dy particle phase has a hcp crystalline structure with the lattice constants of $a = 0.615$ nm and $c = 1.010$ nm and the irregular (Mg, Zn)$_x$Dy particle phase has a fcc crystalline structure with the lattice constant of $a = 0.7423$ nm, respectively. Fig. 9 shows the typical TEM images and corresponding SAED patterns of the rectangular-shaped particle phases and fine lamellar phase in the aged Mg–2Dy–0.5Zn alloy at 80 h. For the SAED pattern of the fine lamellar phase in Fig. 9(c), the incident electron beam is parallel to $[1\,1\,\bar{2}\,0]_{Mg}$ direction and exhibits periodic small diffraction spots at the interval of 1/14 of distance between direct spot and $(0\,0\,0\,2)_{Mg}$ reflection. Therefore, the fine lamellar phase can be confirmed to be the 14H LPSO structure with the lattice constants of $a = 0.289$ nm and $c = 3.738$ nm. Moreover, the average chemical composition of the 14H LPSO phase is determined to be Mg–3.45 at.% Zn–6.12 at.% Dy by the EDS analysis, which is different from that of the 14H LPSO phase observed in the $Mg_{96.5}Zn_1Gd_{2.5}$ alloy (Mg–11 ± 1.0 at.% Zn–8 ± 1.0 at.% Gd) [16] and the $Mg_{97}Zn_1Y_2$ alloy (Mg–7 at.% Zn–6 at.% Y) [23]. In addition, the crystalline structure of the rectangular-shaped Mg$_x$Dy particle phase is estimated to be a bcc crystal structure with a lattice constant of $a = 0.7713$ nm. It can be found that the Mg$_x$Dy phase and the Mg_2Dy phase have similar composition and lattice parameters despite small difference in their crystal structure. This difference might be induced by the distortion in stoichiometric composition. Thus, the formula of the rectangular-shaped particle phase can be written as Mg_2Dy. The enlarged TEM images of the fine lamellar phase in the aged alloys at 36 h and 80 h are displayed in Figs. 8(d) and 9(d) for two typical cases. It can be seen that the width of the 14H LPSO phase increases remarkably along the *c*-axis

Table 1
EDS results of the particle phases in Fig. 7 for the aged Mg–2Dy–0.5Zn alloy at 0 h, 36 h and 80 h, respectively.

Element	*A*		*B*		*C*		*D*	
	(wt.%)	(at.)%	(wt.%)	(at.)%	(wt.%)	(at.)%	(wt.%)	(at.%)
Mg	9.08	30.65	65.11	90.72	23.08	66.74	27.07	71.27
Dy	59.65	30.12	28.40	5.92	76.92	33.26	72.93	28.73
Zn	31.27	39.23	6.49	3.36	–	–	–	–
Total	100	100	100	100	100	100	100	100

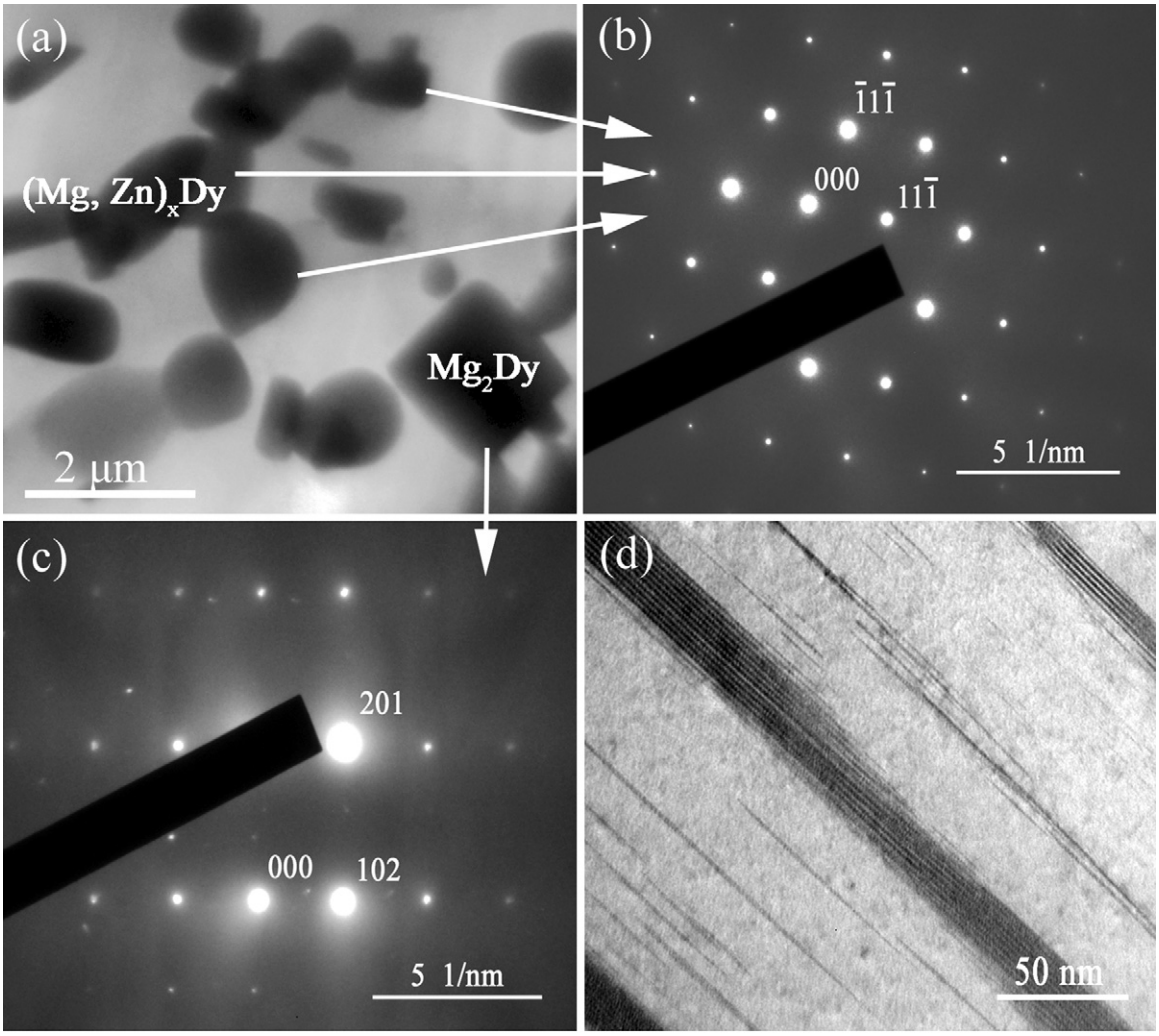

Fig. 8. TEM images of the peak-aged Mg–2Dy–0.5Zn alloy at 36 h (a), the corresponding SAED patterns taken from the irregular particle phase (b) and square-shaped particle phase (c). The corresponding electron beams in the images (b) and (c) are parallel to [0 1 1] and [0 $\bar{1}$ 0], respectively, and the enlarged TEM image of the fine lamellar phase (d) taken from (a).

of the α-Mg matrix and, in contrast, the average spacing of the adjacent 14H LPSO phases decreases significantly with an increase in ageing time from 36 h to 80 h. These results reveal that the 14H LPSO phase forms and grows during ageing.

Despite the homogeneity produced during solid-solution treatment, some local regions enriched in Zn and Dy would exist still. The Zn and Dy atoms in these regions tend to segregate and form the new $(Mg, Zn)_xDy$ particle phases during ageing treatment. It can be seen from Fig. 5(b) that the newly-formed $(Mg, Zn)_xDy$ particle phases distribute mainly in the grain interior and are surrounded by the white transition or depleted regions where the concentrations of Zn and Dy should be lower, while the $(Mg, Zn)_xDy$ particle phases formed during solid-solution treatment distribute mainly at the grain boundaries. The $(Mg, Zn)_xDy$ particle phases formed during solid-solution treatment are in a metastable state and tend to dissolve during ageing. The above two processes develop as ageing time increases and lead to a significant increase in the amount and a more dispersive distribution of the $(Mg, Zn)_xDy$ particle phases at 36 h. As ageing time increases further, the newly-formed $(Mg, Zn)_xDy$ particle phases grow gradually and also start to dissolve like those formed during solid-solution treatment. It can be seen from Fig. 5 (b) and (c) that the newly-formed $(Mg, Zn)_xDy$ particle phases in the grain interior at 36 h have mostly disappeared at 80 h, only those with larger size left. The above dissolution process leads to the decrease in the amount of the $(Mg, Zn)_xDy$ particle phases and also the release of the Zn and Dy atoms into the α-Mg matrix. The latter is favorable for the formation of the 14 H LPSO phase as will be discussed latter.

It has been reported that apart from the transformation from the 18R LPSO phase during solid-solution treatment [23–25], the 14H LPSO phase can also form during ageing process in Mg–Zn–RE alloys [15–17] through a modulated structure-like mechanism [27,28]. The diffusion or segregation of the Zn and RE atoms to the stacking fault planes can enhance the stacking ordering by reducing the stacking fault energy and also can promote the chemical ordering [29,30]. Therefore, the 14H LPSO phase can form and grow in the supersaturated α-Mg solid solution through the diffusions of the RE and Zn atoms during long time ageing treatment. Such formation and growth of the 14H LPSO phase during ageing have been reported for other aged Mg–RE–Zn alloys [15–17]. Moreover, it can be found that the LPSO phase grows mainly along the basal plane and the *c*-axis of the α-Mg matrix [31,32]. Such lateral growth process is obviously easier due to short diffusion distance. For our Mg–2Dy–0.5Zn alloy, the 14H LPSO phase has occupied all the α-Mg grains after solid-solution treatment (Fig. 3(a)). During ageing, the Dy and Zn atoms diffuse slowly in the α-Mg super-saturated solid solution and some of them enrich on the stacked planes, which provides the chemical order for the formation and growth of the 14H

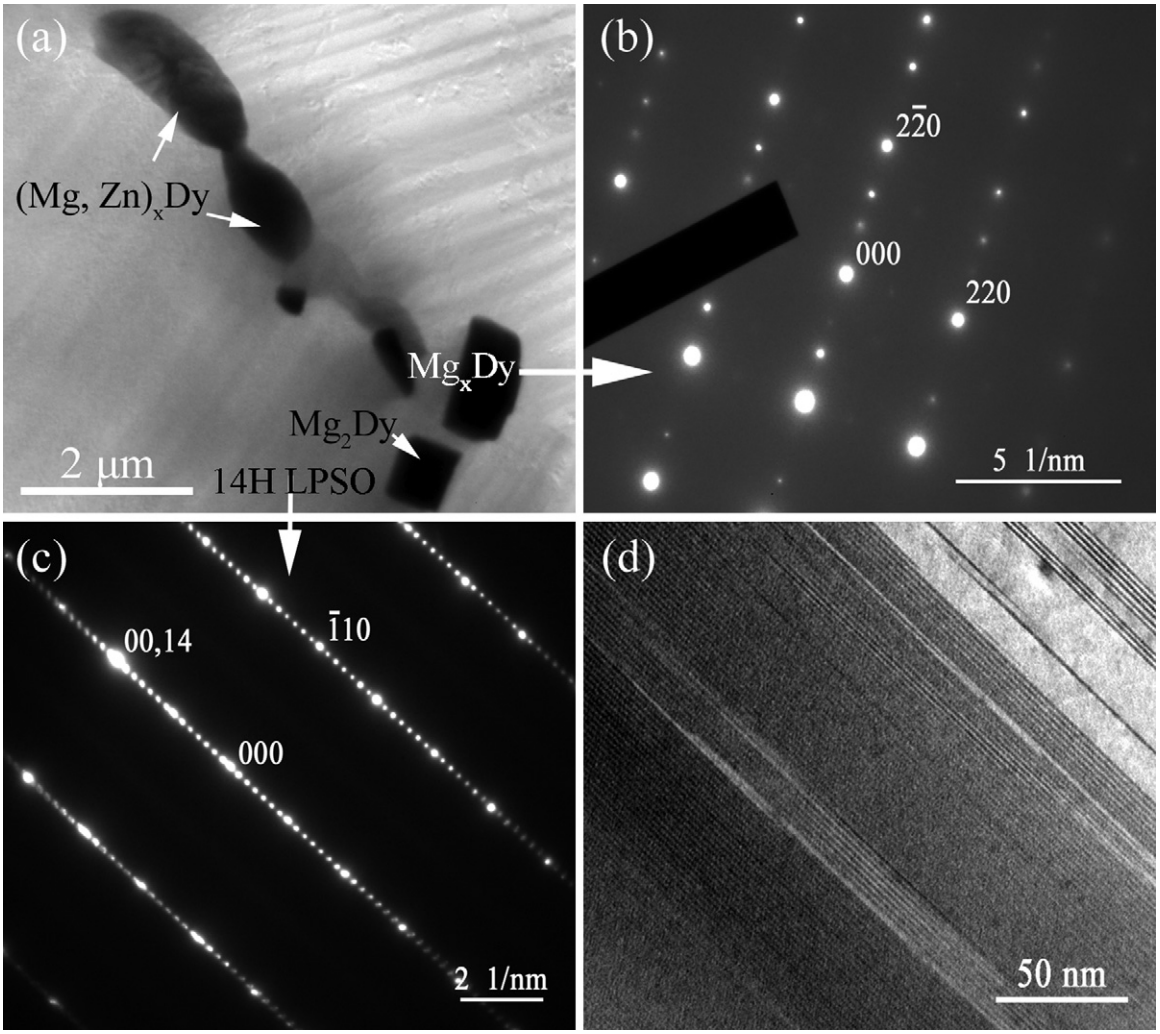

Fig. 9. TEM images of the peak-aged Mg–2Dy–0.5Zn alloy at 80 h (a), the corresponding SAED patterns taken from the rectangular-shaped particle phase (b) and lamellar phase (c). The corresponding electron beams in the images (b) and (c) are parallel to [0 0 1] and [1 1 $\bar{2}$ 0], respectively, and the enlarged TEM image of the fine lamellar phase (d) in taken from (a).

LPSO phase. Furthermore, the small distance between two bundles of the 14H LPSO phase is also a favorable factor in accelerating the diffusions of the Dy and Zn atoms and thus leading to the rapid growth of the 14H LPSO phase in the α-Mg matrix. Besides the high supersaturation in Dy and Zn of the α-Mg matrix, the additional Zn and Dy atoms released due to the dissolution of the (Mg, Zn)$_x$Dy particle phases is also an important factor in promoting the formation and growth of the 14H LPSO phase during ageing. As a consequence, a high volume fraction of the 14H LPSO phase is expected at 80 h.

3.4. Explanation of double-peak ageing behavior

The double-peak ageing behavior observed for the Mg–2Dy–0.5Zn alloy can be explained by the change in the contributions of the precipitation strengthening of the (Mg, Zn)$_x$Dy particle phases and the LPSO strengthening of the 14H LPSO phase. The increased hardness before 36 h arises mainly from the increased contribution of the precipitation strengthening due to the increase in the amount of the (Mg, Zn)$_x$Dy particle phases and their more dispersive distribution in the α-Mg matrix. Therefore, the first ageing hardening peak is mainly related to the precipitation strengthening caused by the (Mg, Zn)$_x$Dy particle phases. Besides the contribution of the precipitation strengthening, the LPSO strengthening of the 14H LPSO phase does also some contribution to the first ageing peak at 36 h, but its contribution is relatively small due to the relatively small amount of the 14H LPSO phase.

The contribution of the precipitation strengthening becomes gradually small as ageing time increases due to the increase in the size and the decrease in the amount of the (Mg, Zn)$_x$Dy particle phases. This suggests that the increased contribution of the LPSO strengthening of the 14H LPSO phase is a possible mechanism responsible for the second ageing peak at 80 h. It has been suggested that the strengthening role of the LPSO phase in Mg alloys comes first from the suppression of the hard LPSO phase on the dislocation activity in the α-Mg matrix [29,33]. The second strengthening role of the LPSO phase arises from the refinement or fragmentation of the LPSO phase through the formation of the kink bands and kink boundaries and the rotation of the formed LPSO blocks, the increased dislocation density in these kinking deformation regions would lead to the additional strengthening during deformation [34]. The third strengthening role of the LPSO phase is attributed to the composite strengthening in which the LPSO phase acts as the reinforcement and its contribution to the strengthening would follow the mixture law of two phase materials [35]. The

above three strengthening roles of the LPSO phase can be enhanced when its amount is increased. Therefore, the second ageing peak observed in our Mg–2Dy–0.5Zn alloy at 80 h should arise from the LPSO strengthening caused by the high volume fraction of the 14H LPSO phase and the precipitation strengthening of the $(Mg, Zn)_xDy$ particle phases although its contribution would be smaller than that at 36 h due to the increase in their size and the decrease in their amount. In addition, the higher thermal stability of the 14H LPSO phase [31,32] can also restrain effectively the grain growth so that the strengthening role of the grain refinement can be maintained during ageing process.

4. Conclusions

The ageing behavior of Mg–2Dy–0.5Zn alloy was investigated during isothermal ageing at 180 °C. Two significant ageing peaks were observed at 36 h and 80 h, respectively. The microstructure examination showed that the as-cast alloy consists of the α-Mg matrix, lamellar $Mg_{12}ZnDy$ phase with 18R LPSO structure and Mg_2Dy particle phase. During the solid-solution treatment at 525 °C for 10 h, the 14H LPSO phase forms through the transformation from the 18R LPSO phase and the dispersion from the supersaturated α-Mg solid solution, the $(Mg, Zn)_xDy$ phase precipitates in the α-Mg matrix. During ageing, the 14H LPSO phase forms and grows from the supersaturated α-Mg solid solution and its volume fraction increases, the size, distribution and amount of the $(Mg, Zn)_xDy$ particle phases change as ageing time increases. The precipitation strengthening and the LPSO strengthening are two main mechanisms responsible for the observed double-peak ageing behavior. The first ageing peak is mainly attributed to the precipitation strengthening of a large amount of the fine $(Mg, Zn)_xDy$ particle phases. The second ageing peak arises mainly from the LPSO strengthening caused by a high volume fraction of the 14H LPSO phase.

Acknowledgements

This work was financially supported by the National Nature Science Foundations of China (No. 50771049 and No. 50871046). The authors would like to express their thanks to D. Zhou, W. Zhang, S. Li and D. Liu for their assistance in some experiments.

References

[1] L.L. Rokhlin, Mg Alloys Containing Rare Earth Metals, Taylor & Francis, London, 2003, p. 1.
[2] B.L. Mordike, T. Ebert, Mater. Sci. Eng. A 302 (2001) 37–45.
[3] Y. Kawamura, K. Hayashi, A. Inoue, T. Masumoto, Mater. Trans. 42 (2001) 1172–1176.
[4] J.F. Nie, X. Gao, S.M. Zhu, Scripta Mater. 53 (2005) 1049–1053.
[5] M. Yamasaki, T. Anan, S. Yoshimoto, Y. Kawamura, Scripta Mater. 53 (2005) 799–803.
[6] Y. Kawamura, M. Yamasaki, Mater. Trans. 48 (2007) 2986–2992.
[7] J. Yang, L.D. Wang, L.M. Wang, H.J. Zhang, J. Alloys Compd. 459 (2008) 274–280.
[8] X.B. Liu, R.S. Chen, E.H. Han, J. Alloys Compd. 465 (2008) 232–238.
[9] T. Homma, N. Kunito, S. Kamado, Scripta Mater. 61 (2009) 644–647.
[10] P. Pérez, G. Garcés, P. Adeva, J. Alloys Compd. 491 (2010) 192–199.
[11] G.L. Bi, D.Q. Fang, L. Zhao, J.S. Lian, Q. Jiang, Z.H. Jiang, Mater. Sci. Eng. A 528 (2011) 3609–3614.
[12] K. Liu, J. Meng, J. Alloys Compd. 509 (2011) 3299–3305.
[13] D.D. Yin, Q.D. Wang, Y. Gao, C.J. Chen, J. Zheng, J. Alloys Compd. 509 (2011) 1696–1704.
[14] J.H. Zhang, Z. Leng, S.J. Liu, J.Q. Li, M.L. Zhang, R.Z. Wu, J. Alloys Compd. (2011), doi:10.1016/j.jallcom.2011.03.059.
[15] T. Honma, T. Ohkubo, S. Kamado, K. Hono, Acta Mater. 55 (2007) 4137–4150.
[16] M. Yamasaki, M. Sasaki, M. Nishijima, K. Hiraga, Y. Kawamura, Acta Mater. 55 (2007) 6798–6805.
[17] K. Liu, J.H. Zhang, D.X. Tang, L.L. Rokhlinc, F.M. Elkinc, J. Meng, Mater. Chem. Phys. 117 (2009) 107–112.
[18] D.J. Li, X.Q. Zeng, J. Dong, C.Q. Zhai, W.J. Ding, J. Alloys Compd. 468 (2009) 164–169.
[19] F.O. Méar, D.V. Louzguine-Luzgin, A. Inoue, J. Alloys Compd. 496 (2010) 149–154.
[20] X.H. Shao, Z.Q. Yang, J.H. You, K.Q. Qiu, X.L. Ma, J. Alloys Compd. (2011), doi:10.1016/j.jallcom.2011.04.067.
[21] S Zhang, G.Y. Yuan, C. Lu, W.J. Ding, J. Alloys Compd. 509 (2011) 3515–3521.
[22] Z.P. Luo, J. Mater. Sci. Lett. 19 (2000) 813–815.
[23] T. Itoi, T. Seimiya, Y. Kawamura, M. Hirohashi, Scripta Mater. 51 (2004) 107–111.
[24] Y.M. Zhu, M. Weyland, A.J. Morton, K. Oh-ishi, K. Hono, J.F. Ni, Scripta Mater. 60 (2009) 980–983.
[25] Y.M. Zhu, A.J. Morton, J.F. Nie, Acta Mater. 58 (2010) 2936–2947.
[26] W.L. Xiao, S.S. Jia, J.L. Wang, J. Yang, L.M. Wang, Acta Mater. 56 (2008) 934–941.
[27] W.J. Ding, Y.J. Wu, L.M. Peng, X.Q. Zeng, G.Y. Yuan, J. Mater. Res. 24 (2009) 1842–1854.
[28] Y.J. Wu, D.L. Lin, X.Q. Zeng, L.M. Peng, W.J. Ding, J. Mater. Sci. 44 (2009) 1607–1612.
[29] E. Abe, Y. Kawamura, K. Hayashi, A. Inoue, Acta Mater. 50 (2002) 3845–3857.
[30] M. Suzuki, T. Kimura, J. Koike, K. Maruyama, Mater. Sci. Eng. A 387–389 (2004) 706–709.
[31] A. Ono, E. Abe, T. Itoi, M. Hirohashi, M. Yamasaki, Y. Kawamura, Mater. Trans. 49 (2008) 990–994.
[32] J. Lee, K. Sato, T.J. Konno, K. Hiraga, Mater. Trans. 50 (2009) 222–225.
[33] Y. Chino, M. Mabuchi, S. Hagiwara, H. Iwasaki, A. Yamamoto, H. Tsubakino, Scripta Mater. 51 (2004) 711–714.
[34] X.H. Shao, Z.Q. Yang, X.L. Ma, Acta Mater. 58 (2010) 4760–4771.
[35] K. Hagihara, A. Kinoshita, Y. Sugino, M. Yamasaki, Y. Kawamura, H.Y. Yasuda, Y. Umakoshi, Acta Mater. 58 (2010) 6282–6293.